Journal of Engineering and Technology for Industrial Applications

ISSN ONLINE: 2447-0228

ITEGAM-JETIA

Manaus, v.11 n.51, p. 197-205. January/February., 2025.

DOI: https://doi.org/10.5935/jetia.v11i51.1456

RESEARCH ARTICLE OPEN ACCESS

ARTIFICIAL NEURAL NETWORK-BASED DEADBEAT PREDICTIVE CURRENT CONTROL WITH DEAD-TIME COMPENSATION FOR PMSMs

Amira Slimani [1*], Amor Bourek [2] , Abdelkarim Ammar [3] , Khoudir Kakouche [4], Wassila Hattab[5], and Marah Bacha [6]

[1,2,3,5,6] dept. Electrical Engineering-LGEB Lab, Biskra University Biskra, Algeria
[3] Institute for Electrical and Electronics Engineering -LSS Lab Boumerdes University Boumerdes, Algeria
[4] Université de Bejaia, Faculté de Technologie, Laboratoire de Technologie Industrielle et de l'Information, Bejaia 06000, Algeria.

[1]http://orcid.org/0009-0009-3259-5743, [2]http://orcid.org/0000-0001-8885-0488, [3]http://orcid.org/0000-0002-6054-9797
[4]http://orcid.org/0000-0001-6365-5029, [5]http://orcid.org/0009-0004-7004-5092, [6]http://orcid.org/0000-0002-5609-3766

Email: amira.slimani@univ-biskra.dz , a.bourek@univ-biskra.dz , a.ammar@univ-boumerdes.dz , khoudir.kakouche@univ-bejaia.dz, wassila.hattab@univ-biskra.dz , marah.bacha@univ-biskra.dz

ARTICLE INFO

Article History
Received: December 09, 2024
Revised: January 20, 2025
Accepted: January 25, 2025
Published: February 28, 2025

Keywords:
PMSM
ANN-DPCC
Dead time compensation
Minimizing current distortions.

ABSTRACT

In the velocity control of Permanent Magnet Synchronous Motors (PMSMs), Deadbeat Predictive Current Controllers (DPCCs) are renowned for their excellent dynamic performance and constant switching frequency. However, achieving precise velocity regulation remains challenging due to the nonlinearities introduced by two-level voltage source inverter (2L-VSI). Specifically, the dead time inherent in 2L-VSI results in voltage distortion, which generates parasitic harmonics in the system. These harmonics degrade control accuracy, cause a current ripple, and can lead to performance degradation or even system instability, compromising reliable operation. This article proposes an innovative solution: Artificial Neural Network-Based Deadbeat Predictive Current Control (ANN-DPCC) integrated with dead-time compensation to address these issues. This approach effectively suppresses the current ripple and significantly reduces total harmonic distortion (THD). Simulation results validate that ANN-DPCC with dead-time compensation outperforms traditional DPCC by improving response times, enhancing steady-state accuracy, and minimizing current distortions. This novel strategy significantly advances PMSM control, offering precise velocity regulation, improved reliability, and superior system performance for demanding applications

I. INTRODUCTION

PMSMs have gained widespread attention due to their remarkable characteristics, including compact design, high efficiency, and exceptional power density [1],[2]. These advantages have led to their extensive application in various fields, such as robotics, intelligent manufacturing, and automotive drive systems, where they play a vital role in advancing technological progress in the manufacturing industry [3].

As motor design and manufacturing evolve, the need for more efficient and reliable control strategies for PMSMs has become increasingly important. Conventional control strategies have been widely implemented, including Direct Torque Control (DTC) and Field-oriented Control (FOC). However, in recent years, predictive control techniques have emerged as a promising alternative, offering enhanced performance in motor drive systems and power electronics [4-6].

Predictive control has gained popularity in motor control applications due to its ability to effectively manage multi-objective optimization and constraint problems without requiring parameter adjustments [7],[8]. This approach forecasts state variables' future behavior using the mathematical model of the system. Analyzing cost functions helps the controller choose the best voltage vector and implement it in the system. Commonly employed among the several predictive control strategies in motor drive systems are Deadbeat Predictive Control (DPC) and Finite Control Set Model Predictive Control (FCS-MPC) [9],[10].

Among the various predictive control techniques, DPC has gained popularity due to its ability to deliver superior steady-state

performance, including smoother current waveforms and reduced torque ripple, which significantly improve system stability [11], [12]. We can further categorize the deadbeat control method into Deadbeat Predictive Current Control and Deadbeat Direct Flux and Torque Control (DB-DTFC) [13]. While DB-DTFC requires complex flux and torque observers, DPCC simplifies the process by directly predicting and controlling the current, making it ideal for applications where current regulation is the primary focus [14]. The DPCC technique computes the voltage command for current tracking based on a discrete motor model. Then, it applies Space Vector Pulse Width Modulation (SVPWM) to convert the voltage command into the corresponding switching states [15],[16].

However, performance degradation in the DPCC of PMSM systems can be caused by two main issues. Traditional proportional-integral (PI) speed controllers in DPCC typically exhibit positive steady-state performance. Still, they are vulnerable to parameter variations like load changes and speed fluctuation. Another significant problem arises in two-level voltage source inverters (2L-VSI) fed PMSM systems because of the dead time created by SVPWM switching operations [17]. Although this dead time is brief (typically in the microsecond range), it causes voltage distortion, leading to current ripple and torque pulsations that degrade overall motor control performance [18]. Nonlinearities in the 2L-VSI, such as switching delays and voltage drops in the inverter components, cause these distortions. These distortions contribute to harmonic distortion in the motor currents, reducing the effectiveness of traditional vector control algorithms. Without adequate compensation for dead time, the DPCC control performance can further deteriorate, leading to increased losses and reduced PMSM efficiency. To mitigate these adverse effects. One practical approach leverages Fourier series analysis to model the distorted voltage components in a stationary reference frame. These methods improve the quality of the inverter's output and the accuracy of tracking reference control signals by finding and canceling out the harmonic components caused by dead time [19].

Furthermore, DPCC ability to dynamically predict and adjust inverter output voltages has led to its widespread adoption. By integrating dead-time compensation into the DPCC framework, the system can correct real-time voltage errors, significantly reducing current ripple and total harmonic distortion. This improves the precision of control signals and ensures smoother torque output, making the method highly effective for applications requiring high performance and robustness.

The primary contribution of this paper lies in developing a DPCC strategy enhanced with an ANN-based speed controller to significantly improve the dynamic performance of the speed outer loop in PMSMs. This work also integrates dead-time compensation to address the challenges associated with voltage distortions and torque pulsations in VSI-fed systems. The key contributions are summarized as follows:

1-A neural network replaces the conventional PI controller in the speed control loop. This substitution enhances reference speed tracking, improves adaptation to load variations and speed fluctuations, and results in a superior dynamic response.

2-The proposed DPCC method enables precise current tracking and rapid response by predicting the system's behavior and minimizing tracking errors in both speed and current. This enhances dynamic performance and improves overall system efficiency.

3- The integration of dead-time compensation effectively mitigates the adverse effects of switching delays in VSI-fed PMSM systems. This approach reduces voltage distortions, minimizes current ripple, and improves torque smoothness, enhancing the motor's control accuracy and efficiency. The rest of the paper is organized as follows: Section II presents the mathematical model, including the inverter and PMSM models. Section III details the proposed control method. It consists of two main steps: the current inner loop, which includes deadbeat predictive current control and the proposed dead-time compensation method, and the speed outer cloop, which incorporates artificial neural networks. Section IV demonstrates the simulation results, verifying the effectiveness of the proposed method. Section V concludes the entire paper.

II. MATHEMATICAL MODEL

The ANN-DPCC strategy with dead-time compensation is implemented for a PMSM powered by a 2L-VSI, as illustrated in Figure. 1(a). This section presents the mathematical models for the power converter and the PMSM, forming the foundation for the proposed control approach.

II.1 INVERTER MODEL

The switching state S_x for the 2L-VSI is given by the following relations [20]:

$$S_x = \begin{cases} 1 & if\ G_x\ turn-on\ \ and\ \ \bar{G}_x\ turn-off \\ 0 & if\ G_x\ turn-off\ \ and\ \ \bar{G}_x\ turn-on \end{cases} \quad (1)$$

For $x \in (a,b,c)$, G_x and $\bar{G}_x$ denotes the gate signals of the upper and lower IGBTs, respectively. The voltage combinations at the inverter's output terminals can be expressed using vector representation:

$$V = V_{dc}.\frac{2}{3}(S_a + aS_b + a^2S_c) \quad (2)$$

Where: V is the voltage combinations, V_{dc} is the dc-link voltage, and $a = e^{j\frac{2\pi}{3}}$

The inverter has eight possible switching state combinations, as described in Equation (3), resulting in eight distinct voltage vectors as shown in Fig. 1(b) [1].

$$S_{abc} = (S_a, S_b, S_c) \in V_i = \{000, 001, \ldots\ldots, 111\} \quad (3)$$

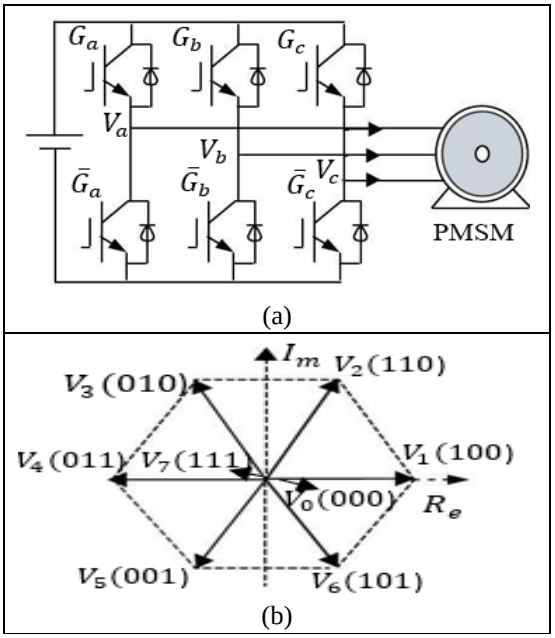

Figure 1: Two-Level Voltage Source Inverter (2L-VSI) .(a) Power Circuit Diagram, and (b) Voltage Vector Representation.
Source: Authors, (2025).

II.2 PMSM MODEL

The mathematical representation of a PMSM voltage equation in the rotating $(d-q)$ reference frame can be represented as [21], [10]:

$$\begin{cases} U_{sd} = R_s I_{sd} + L_d \frac{dI_{sd}}{dt} - L_q \omega_e I_{sq} \\ U_{sq} = R_s I_{sq} + L_d \frac{dI_{sq}}{dt} + -L_q \omega_e I_{sd} + \varphi_f \omega_e \end{cases} \quad (4)$$

Where U_{sd} and U_{sq} are the stator input voltage, R_s is the stator resistance, I_{sd} and I_{sq} are the stator currents, φ_f is the flux linkages, L_d and L_q are the stator inductances, respectively, (L_d=L_q=L_s) for the surface-mounted permanent magnet synchronous moto.

Additionally, ω_e is the rotor electrical angular speed, calculated as $(\omega_e = \mathrm{p} * \omega_m)$, where ω_m represents the rotor's mechanical rotational speed, and p is the number of poles.

III. PROPOSED CONTROL METHOD

The control strategy framework, depicted in figure 2 comprises two main stages: the current inner loop and the speed outer loop. The current inner loop precisely manages the stator currents in the electrical subsystem for accurate current control. The DPCC strategy is made better by dead-time compensation in the 2L-VSI.

Meanwhile, the speed outer loop manages the machine's mechanical subsystem using an ANN instead of traditional PI controllers. This loop tracks the speed reference accurately by employing the mechanical model to determine an appropriate electromagnetic torque reference (T_e^*).

III.1 DEADBEAT PREDICTIVE CURRENT CONTROL

The primary forward-order Euler discretization obtains the subsequent instantaneous stator currents. At the (k) th moment, the stator currents on the d-q axis, $I_{sd}(k)$, and $I_{sq}(k)$, are sampled to predict the currents at the $(k+1)$th moment [22],[23].

$$\begin{cases} I_{sd}(k+1) = \left(1 - \frac{R_s T_s}{L_d}\right) I_{sd}(k) + T_s \omega_e(k) I_{sq}(k) + \frac{T_s}{L_d} U_{sd}(k) \\ I_{sd}(k+1) = \left(1 - \frac{R_s T_s}{L_d}\right) I_{sq}(k) - T_s \omega_e(k) I_{sd}(k) - \frac{T_s \varphi_f}{L_d} \\ \omega_e(k) + \frac{T_s}{L_d} U_{sq}(k) \end{cases} \quad (5)$$

Where: $U_{sd}(k)$, and $U_{sq}(k)$ signify the d-q axis stator voltages at the (k)th moment, while $I_{sd}(k)$, and $I_{sq}(k)$ denote the d-q axis stator currents at the same instant. $I_{sd}(k+1)$ and $I_{sq}(k+1)$ denote the expected stator currents at the $(k+1)$th instant, $\omega_e(k)$ represents the electrical angular velocity at the (k) th instant, and T_s refers to the sampling time.

The reference currents $I_{sd}^*(k)$ and $I_{sq}^*(k)$ in the d-q rotating coordinate system can exhibit slight variation between two consecutive time intervals, provided the sampling duration is sufficiently small. This attribute of reference currents is denoted as:

$$\begin{aligned} I_{sd}^*(k+1) &\approx I_{sd}^*(k) \\ I_{sq}^*(k+1) &\approx I_{sq}^*(k) \end{aligned} \quad (6)$$

The second step aims to calculate the specified voltage at the (k +1) th instant, which can be expressed as:

$$\begin{cases} U_{sd}(k+1) = R_s I_{sd}(k+1) + \frac{L_s}{T_c}[I_{sd}^*(k) - I_{sd}(k+1)] - L_s \\ \omega_e I_{sq}(k) \\ U_{sq}(k+1) = R_s I_{sq}(k+1) + \frac{L_s}{T_c}\left[I_{sd}^*(k) - I_{sq}(k+1)\right] - L_s \omega_e \\ I_{sd}(k) + \varphi_f \omega_e \end{cases} \quad (7)$$

III.2 PROPOSED DEAD-TIME COMPENSATION METHOD

Figure 3. a illustrates the ideal and actual gate signal patterns, accounting for dead time. Figure 3. b displays the ideal and actual a-phase voltages according to the phase current direction. Over one SVPWM period T_s , the voltage distortion error in the a-phase due to dead time can be represented as follows [24].

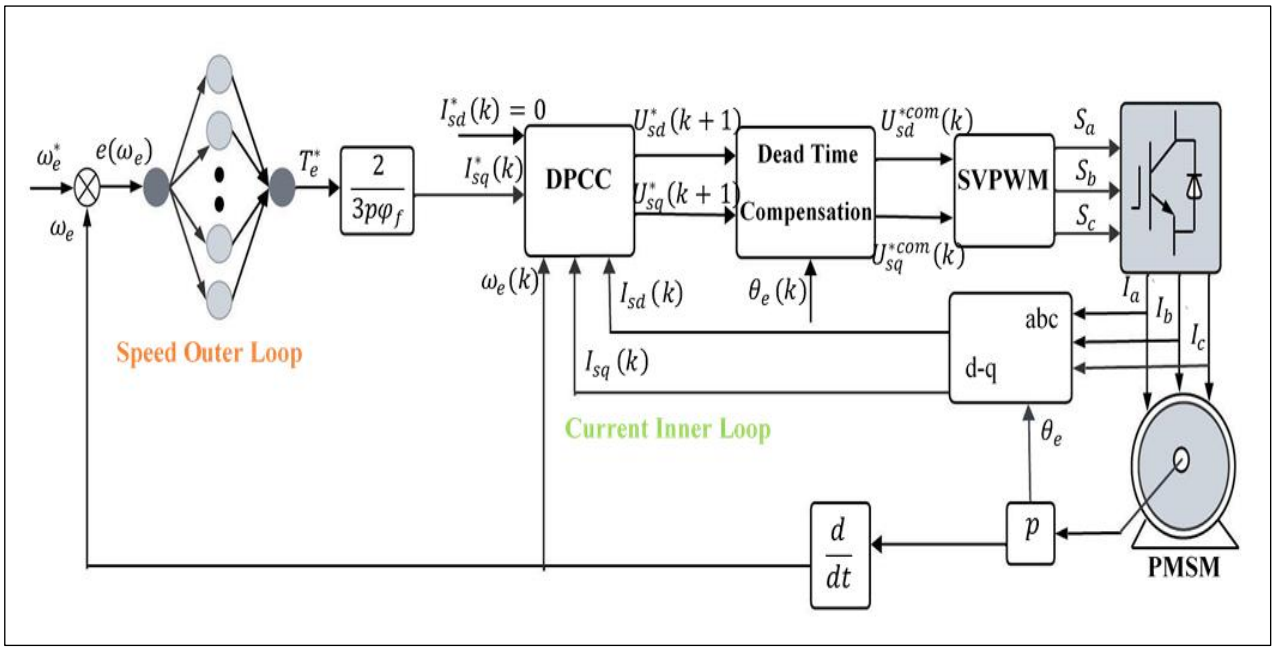

Figure 2: schematic Representation of ANN-DPCC with Dead-Time Compensation in PMSM Drives.
Source: Authors, (2025).

$$\Delta V_{ap} = V_{DT} sign(I_a) \qquad sign(I_a) = \begin{cases} 1 & I_a > 0 \\ -1 & I_a < 0 \end{cases} \quad (8)$$

Where: sign (.) is sign function. In equation (9), V_{DT} is the magnitude of the voltage error due to dead-time,which can be given as follows:

$$V_{DT} = \frac{V_{DT} + T_{on} - T_{off}}{T_s} . (V_{dc} - V_{ce} + V_D) + \frac{V_{ce} + V_D}{T_s} \quad (9)$$

Where T_{DT} denotes the dead time, T_{on} represents the switching turn-on time., T_{off} is the switching turn-off time, V_{ce} is the forward voltage drop of the switching device, and V_d represents the forward voltage drop of the diode. In this case, the voltage drops across the switching and diodes are neglected, simplifying equation (10) to:

$$V_{DT} = \frac{V_{DT} + T_{on} - T_{off}}{T_s} \quad (10)$$

The voltage error can be converted into an $\alpha - \beta$ reference frame using equation (11), as illustrated in Figure 3.b.

$$\begin{bmatrix} \Delta U_{s\alpha} \\ \Delta U_{s\beta} \end{bmatrix} = \begin{bmatrix} \frac{2}{3} & -\frac{1}{3} & -\frac{1}{3} \\ 0 & \frac{1}{\sqrt{3}} & -\frac{1}{\sqrt{3}} \end{bmatrix} \begin{bmatrix} V_{DT}.sign(I_a) \\ V_{DT}.sign(I_b) \\ V_{DT}.sign(I_c) \end{bmatrix} \quad (11)$$

The voltage error $\Delta U_{s\alpha\beta}$ you can obtain an estimate by converting it into a Fourier series [25]:

$$\begin{cases} \Delta U_{s\alpha} = \frac{4\,V_{DT}}{\pi} [\sin(\theta_e + \varphi) + \sum_{n=1}^{\infty} \frac{\sin\left((6n-1)(\theta_e+\varphi)\right)}{6n-1} + \\ \qquad \frac{\sin\left((6n+1)(\theta_e+\varphi)\right)}{6n+1}] \\ \Delta U_{\beta} = \frac{4\,V_{DT}}{\pi} [\cos(\theta_e + \varphi) + \sum_{n=1}^{\infty} \frac{\cos\left((6n-1)(\theta_e+\varphi)\right)}{6n-1} + \\ \qquad \frac{\cos\left((6n+1)(\theta_e+\varphi)\right)}{6n+1} \end{cases} \quad (12)$$

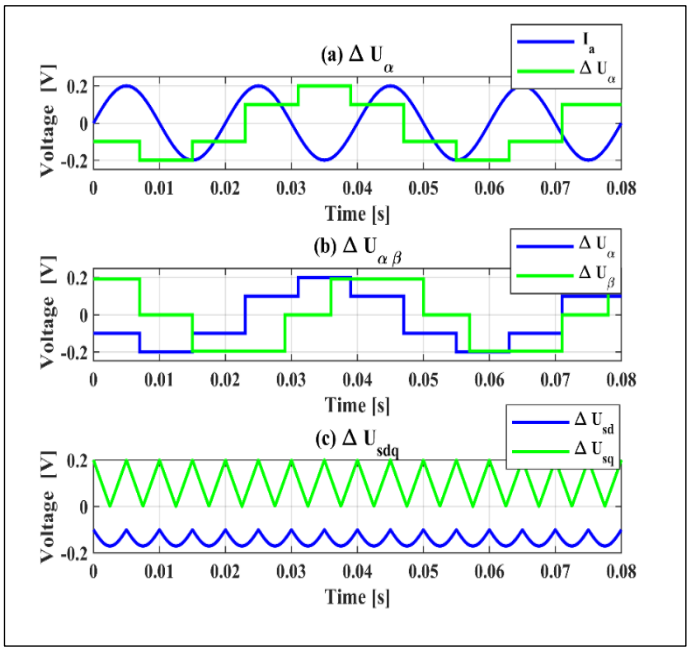

Figure 3. Illustration of voltage distortions.
Source: Authors, (2025).

In this context, φ denotes the angular difference between the current vector in the $(d-q)$ reference frame and the q -axis. Due to dead-time effects, the appearance of 5th and 7th harmonic components in the voltages becomes evident, as shown by the harmonic analysis in Equation (12). As demonstrated in equation (13), these harmonics are mapped to multiples of the 6 th harmonic in the $(d-q)$ reference frame. The resulting disturbance voltages $\Delta U_{s,dq}$ are illustrated in Figure 3.c

$$\begin{cases} \Delta U_{sd} = \frac{4\,V_{DT}}{\pi} [\sin(\varphi) + \sum_{n=1}^{\infty} \frac{\sin(6n(\theta_e+\varphi)-\varphi)}{6n-1} + \\ \qquad \frac{\sin(6n(\theta_e+\varphi)+\varphi)}{6n+1}] \\ \Delta U_{sd} = \frac{4\,V_{DT}}{\pi} [-\cos(\varphi) + \sum_{n=1}^{\infty} \frac{\cos(6n(\theta_e+\varphi)-\varphi)}{6n-1} + \\ \qquad \frac{\cos(6n(\theta_e+\varphi)\mp\varphi)}{6n+1}] \end{cases} \quad (13)$$

The harmonic ripple of the current $I_{s,\alpha\beta}$ and current $I_{s,dq}$ at the same frequencies is caused by these harmonic components in the voltage. We can mitigate the undesirable effects of the dead time and the other VSI nonlinearities by adequately compensating. The dead-time compensation method adjusts the reference voltage $U_{s,dq}^{*com}(k)$ by adding or subtracting the dead-time-induced voltage ΔU_{sdq}, depending on the direction of the q-axis reference current $I_{sq}^{*}(k)$ and the rotor speed ω_e, can be represented as:

$$\begin{cases} U_{s,dq}^{*com}(k) = U_{s,dq}(k+1) - \Delta U_{s,dq} & if\ \ I_{sq}^{*}(k) \geq 0 \\ U_{s,dq}^{*com}(k) = U_{s,dq}(k+1) + \Delta U_{s,dq} & if\ \ I_{sq}^{*}(k) < 0 \\ \qquad and\ \omega_e(k) < 0 & \\ U_{s,dq}^{*com}(k) = U_{s,dq}(k+1) - \Delta U_{s,dq} & if\ \ I_{sq}^{*}(k) > 0 \\ \qquad and\ \omega_e(k) > 0 & \end{cases} \quad (14)$$

Where : $U_{s,dq}^{*com}(k)$ are the reference compensation voltages on the $d-q$ axis q that are generated by the DPCC controllers, ,calculated for the $k+1$ period. This equation (15) scales the adjusted d-q voltage components if their amplitude exceeds a certain threshold (specifically (V_{dc}/3)) .This scaling helps ensure that the voltage commands remain within the allowable limits of the inverter.

$$\begin{cases} U_{sd}^{*com}(k) = U_{sd}^{*com}(k) V_{dc}/\sqrt{3} \sqrt{\left(U_{sd}^{*com}(k)\right)^2 + U_{sq}^{*com}(k)^2)} \\ U_{sq}^{*com}(k) = U_{sq}^{*com}(k) V_{dc}/\sqrt{3} \sqrt{\left(U_{sd}^{*com}(k)\right)^2 + U_{sq}^{*com}(k)^2)} \end{cases} \quad (15)$$

III.3 THE PRINCIPLE IDEA OF ARTIFICIAL NEURAL NETWORK

ANN technique is a computational model inspired by biological neural systems, designed to emulate human cognitive abilities in machine and control systems. ANNs consist of interconnected nonlinear processing units, or neurons, linked by synapses represented as numerical weights. This structure enables ANNs to overcome the limitations of traditional control methods through adaptive learning and processing. Typically organized into three layers - input, hidden, and output - the ANN framework allows for efficient transmission and transformation of information throughout the network. One of the model's key strengths is its adaptability to internal and external data, enabling it to respond to changing conditions dynamically [26]. The fundamental structure

of a neuron within this model is conceptually represented by the following equation:

$$y_i = F_1(s)(\sum_{i=1}^{N}(x_i w_i + b)) \quad (16)$$

$$O_i = F_2(s)(\sum_{i=1}^{N}(y_i w_i + b)) \quad (17)$$

Where y_i the output signals of the neuron, O_i is the actual response by network, x_i input signals , w_i represents the synaptic weight of the signal, b is the bias parameter, and $F_1(s)$ represents the activation function of the nonlinear hyperbolic tangent, which is calculated using the following formula.

$$F_1(s) = \frac{e^{\alpha s} - e^{-\alpha s}}{e^{\alpha s} + e^{-\alpha s}} \quad (18)$$

The function of linear activation is represented by $F_2(s)$, which can be calculated using equation (19):

$$F_2(s) = s\beta \quad (19)$$

Where the activation functions gains denote α and β, the feedforward backpropagation method trains the neural network in this study until the MSE between the intended output and the network's output is minimal [27]. The following equation is employed to determine the MSE:

$$MSE = \frac{1}{N}(\sum_{i=1}^{N}(d_i(k) + O_i(k))^2 \quad (20)$$

Where $d_i(k)$ denotes the desired response, N denotes the input-output training data and k denotes the number of iterations. The ANN structure implemented in this study is illustrated in Figure 4.

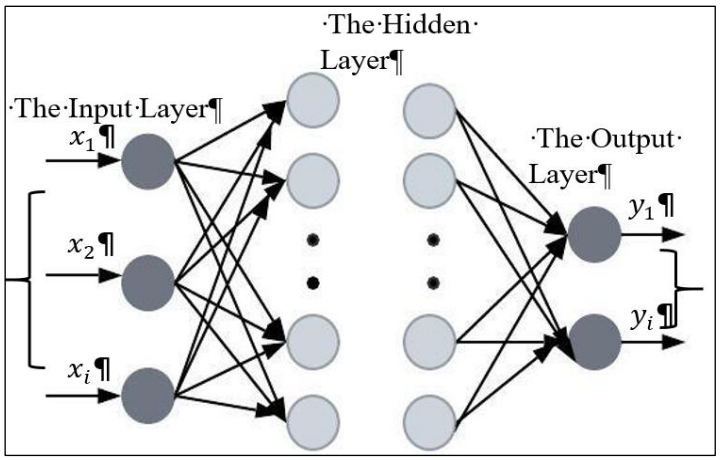

Figure 4. illustrates the structure of the ANN model.
Source: Authors, (2025)

III.3.1 PREPARATION OF INPUT-OUTPUT DATA FOR LEARNING

The first step in this process involves gathering datasets. The dataset includes input and output values from the speed regulator PI, specifically e(w), and T_e^* .We then randomly divide these data into three subsets for training, validation, and testing.

- We designate 70% of the dataset for training.
- We designate 15% of the dataset for testing.
- We reserve 15% of the dataset for validation.

III.3.2 SELECTION OF THE NEURAL NETWORK ARCHITECTURE

Configured the neural network controllers using MATLAB's "nntool" interface. The performance depends on factors such as the number of hidden layer neurons, activation functions, and the training algorithm. A Multi-Layer Perceptron Feedforward architecture, comprising input, hidden layers, and output layers, was selected for this study. Additionally, no standardized methodology exists for selecting the number of hidden layers or neurons. We initially tested single hidden-layer architectures with a small number of neurons, gradually increasing the number of neurons until we achieved the desired performance. After extensive testing, the speed controller's optimal configuration was ten neurons. We applied tangent-sigmoid activation functions (tansig) to the hidden layer and linear activation functions (purelin) to the output layer.

III.3.3 SELECTION OF THE LEARNING ALGORITHM

The final step is selecting the learning algorithm, with the Backpropagation Error Learning Method chosen for this study. MATLAB provides various algorithms, including gradient descent (traingd), gradient descent with momentum (traingdm), and the Levenberg-Marquardt algorithm (trainlm). This study utilized the Levenberg-Marquardt algorithm (trainlm). The Mean Square Error (MSE) and the regression value V are crucial performance indicators. The regression value V measures the correlation between outputs and targets; 1 means a perfect correlation. The errors become acceptable results with weights adjusted iteratively using the Levenberg-Marquardt algorithm.

III.3.4 THE NEURAL NETWORK RESULTS

The MSE as a function of the number of epochs for speed prediction is illustrated in Figure 5. The results suggest a substantial decrease in the error between the objective and predicted output during the training process. The error decreases significantly within the first 1000 epochs, following which it stabilizes, achieving a final RMSE value of approximately 4.44e-5. The optimal specifications of the proposed ANN models are summarized in Table 1.

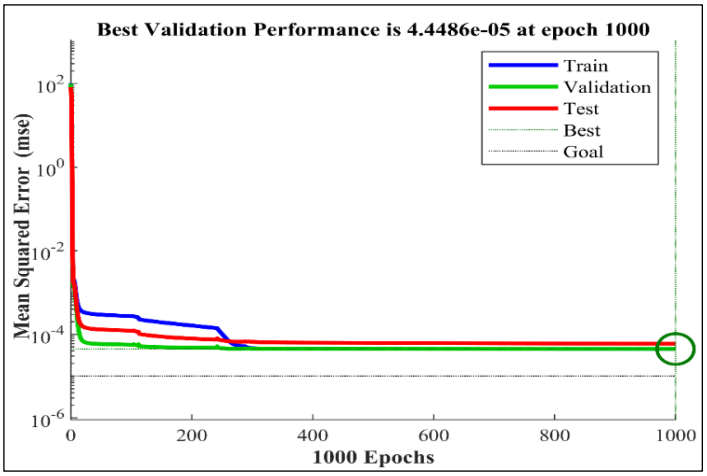

Figure 5. Performance of MSE (Testing, Validation, Training).
Source: Authors, (2025).

Table 1: illustrates the architecture and training parameters of the ANN.

ANN of Parameter	ANN Controller Speed
Neural network	Multi-Layer Perceptron Feedforward
The input layer number of neurons	1
Number of neurons in the hidden layer	10
The output layer number of neurons	1
Learning rate	0.1
Epochs number	1000
ANN training algorithm	Backpropagation
Adaption learning function	Trainlm
Activation function	Tansig
Performance function	MSE 4.44e-5

Source: Authors, (2025).

IV. RESULTS AND DISCUSSIONS

The simulation results were generated using MATLAB/Simulink. The characteristics of the PMSM are detailed in Table 2, which outlines the nominal parameters for a 3 kW power rating. The results are divided into two sections: the first provides a comparative analysis of ANN-DPCC and PI-DPCC performance under sudden load changes in the PMSM. In contrast, the second focuses on the Dead-Time Compensation Strategy applied to PI-DPCC and ANN-DPCC methods.

Table 2: PMSM nominal parameters used in numerical simulation.

Parameters	Values
Stator Inductance *Ls (H)*	0.0076
Stator resistance *Rs* (Ω)	2.3
Friction coefficient *B (N.m.s)*	0.000169
Moment of inertia *J (kg. m^2)*	0.0032
flux linkages $\varphi_f(wb)$	0.4
Number of pole pairs *p*	4

Source: Authors, (2025).

IV.1 DYNAMIC PERFORMANCE OF ANN-DPCC AND PI-DPCC UNDER SUDDEN LOAD CHANGES IN PMSM

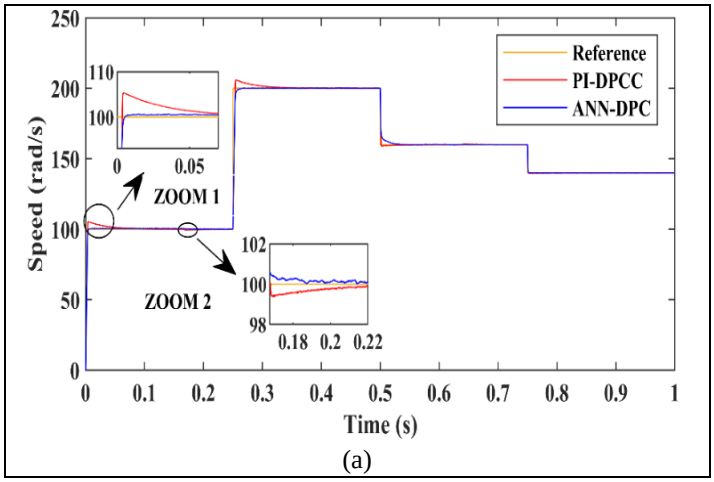

(a)

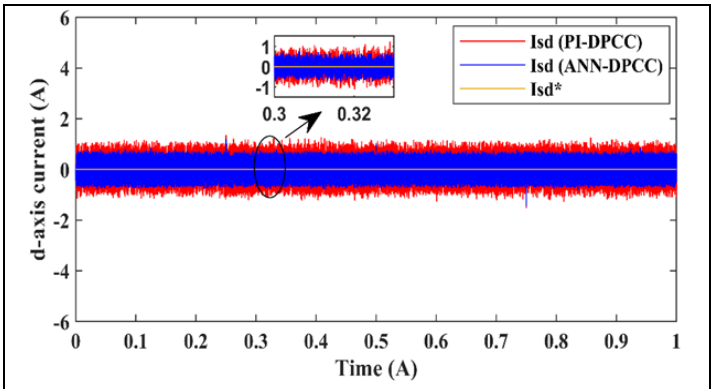

(b)

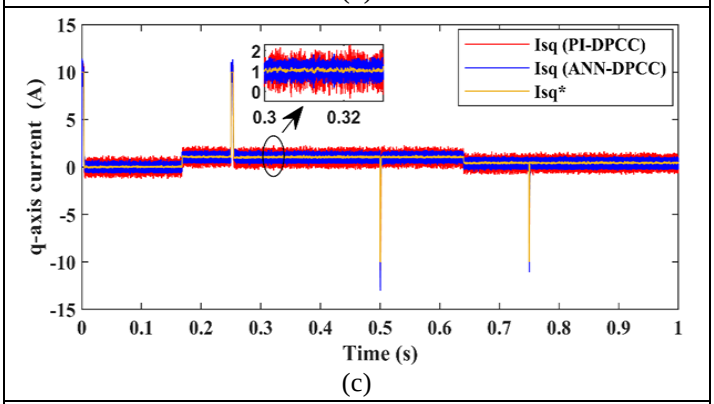

(c)

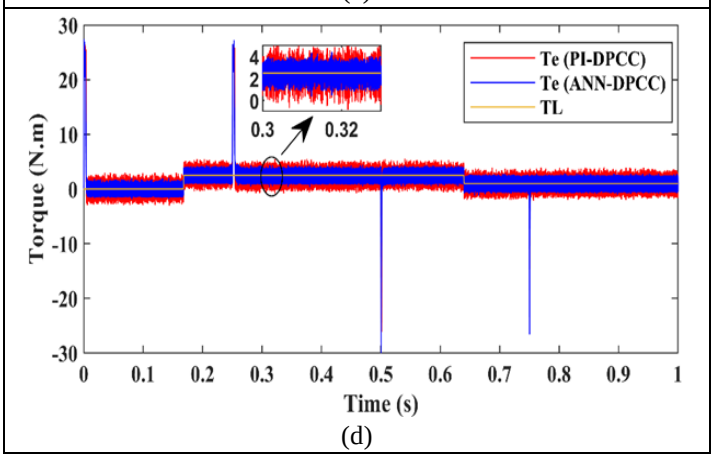

(d)

Figure 6. Performances of the PI-DPCC and ANN-DPCC applied on PMSM drive system : (a) Speed (ω_e), (b) direct current (I_{sd}), (c) quadratic current (I_{sq}), and (d) electromagnetic torque(T_e)
Source: Authors, (2025).

Figure 6.a shows the motor speed profile. According to this figure, the speed starts at 100 rpm, then increases to 200 rpm at 0.25 s, decreases to 160 rpm at 0.5 s, and reduces to 140 rpm at 0.75 s. The measured rotational speed fluctuates based on the reference, with good tracking dynamics observed under no-load and load conditions. Zoom (1) in Figure 6.a reveals that initially, the motor runs at a rated speed of 100 rad/s without load using classical PI-DPCC control, which shows an overshoot of 5.959%. In contrast, there is no overshoot when using the ANN-DPCC control.

The motor's speed regulation response time is 88.87 ms for classical PI-DPCC and ANN-DPCC controller is 5.56 ms, resulting in an improvement of 93.74%. A sudden change in load torque (2.5 Nm) is applied at t = 0.168 s, as shown in Zoom 2. Applying the load, both strategies show an undershoot in speed. The undershoot for PI-DPCC is 0.637 rad/s, while ANN-DTC is 0.2111 rad/s, demonstrating an improvement of 66.87%. The rejection times for classical PI-DPCC and ANN-DPCC are 82 ms and 19.39 ms, respectively. Consequently, ANN-DPCC more effectively preserves the system's speed stability than PI-DPCC, significantly improving the PMSM system's Variation load performance.

Figures 6. b and 6. c display the waveforms of the I_{sd} and I_{sq} current components for the PI-DPCC and ANN-DPCC control strategies. These show how the control method affects the system differently, especially during steady-state and transient conditions. The ANN-DPCC strategy achieves a significant ripple reduction in the I_{sq} current, with values decreasing from 1.164 A in PI-DPCC to 0.455 A, corresponding to an improvement of 60.91%. Similarly, ANN-DPCC minimizes the I_{sd} current ripple by 59.69%, reducing it from 1.310 A for PI-DPCC to 0.528 A.

This enhancement is credited to the neural network integration, which effectively mitigates oscillations and improves control efficiency. Figure 6.d illustrates the electromagnetic torque waveforms for the PI-DPCC and ANN-DPCC techniques. Since the flux remains constant, the behaviour of the electromagnetic torque closely aligns with that of the current. The torque ripple observed with the conventional PI-DPCC is significantly higher, measuring 2.452 Nm, compared to 1.084 Nm with ANN-DPCC, indicating a substantial improvement of 55.79%. The results shown in Table 3 showed that in terms of general performance (dynamics, stability, speed and precision), the ANN-DPCC control outperformed the PI-DPCC control.

Table 3: Evaluating the Characteristics of PI-DPCC and ANN-DPCC

Parameters	Characterstics	PI-DPCC	ANN-DPCC	Improvement (%)
ω_e (rad/s)	**Response time (ms)**	88.87	5.56	93.74
	Overshoot (%)	5.959	0	100
	Rejection time (ms)	82	19.39	76.35
	Undershoot (rad/s)	0.637	0.2111	66.87
$I_{sd}(A)$	**Ripple (A)**	1.310	0.528	59.69
I_{sq} (A)	**Ripple (A)**	1.164	0.455	60.91
$T_e(N.m)$	**Ripple (N.m)**	2.452	1.084	55.79

Source: Authors, (2025).

IV.1 DEAD-TIME COMPENSATION STRATEGY FOR PI-DPCC AND ANN-DPCC METHODS

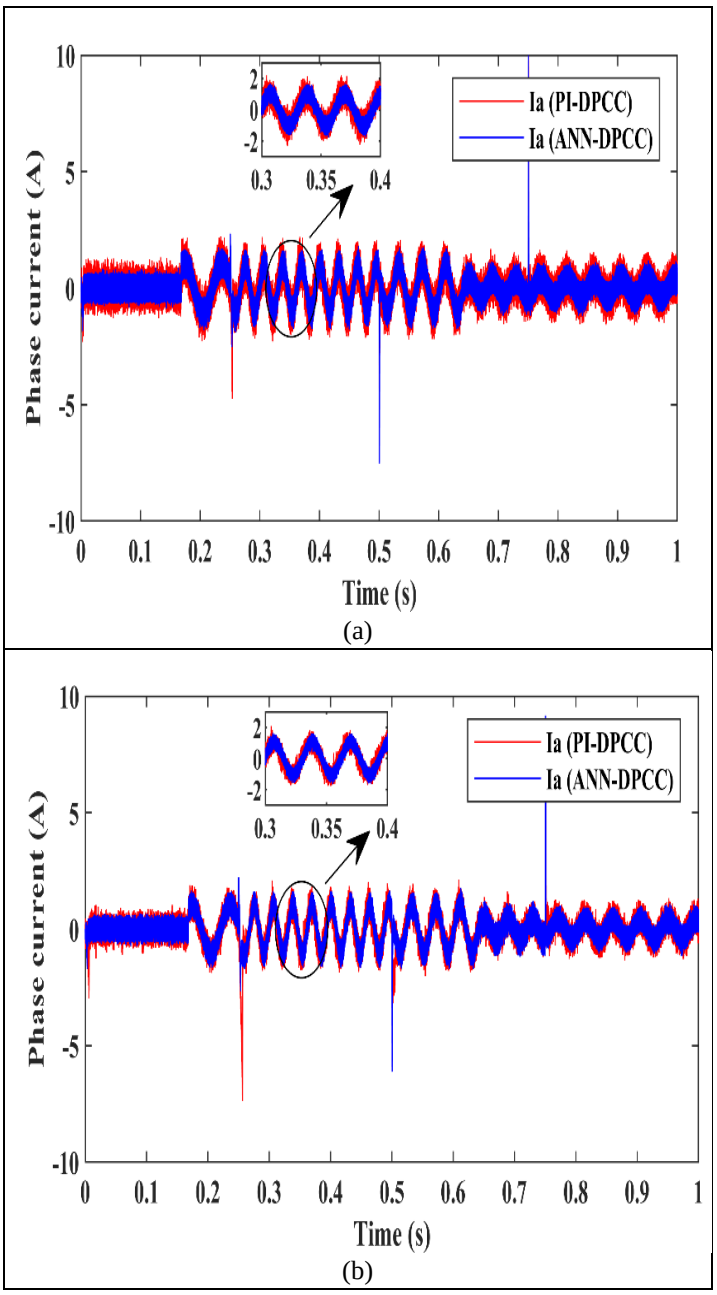

Source: Authors, (2025).

Figure 7: phase current of the PMSM in steady-state. (a) Without dead-time compensation, (b) With dead-time compensation Figures 7.a, and 7.b show the motor operation results with and without the dead-time compensation method. The phase-A current has apparent harmonic distortion when the PI-DPCC method is used for the PMSM system, as shown in Figure 8a. This distortion can negatively affect the operational performance and efficiency of the PMSM system. On the other hand, the ANN-DPCC method significantly reduces the harmonic distortion in the phase-A current. The phase-a current I_a experiences substantial distortion due to dead-time effects in the PI-DPCC system, but this is less pronounced in the ANN-DPCC system. Also, the suggested dead-time compensation method Figure 7.b reduces these problems when the ANN-DPCC control strategy is used. Therefore, dead-time compensation using the ANN-DPCC controller significantly improves the current quality of the PMSM system.

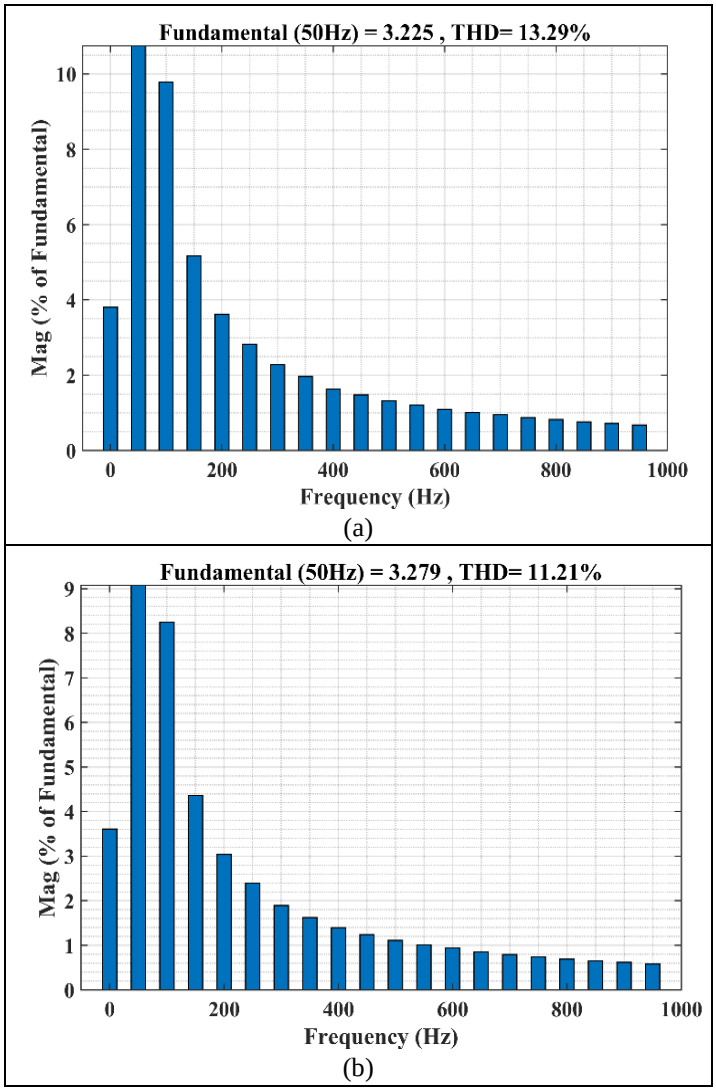

Figure 8: FFT analysis stator current of the PMSM at given state. (a) PI-DPCC. (b) ANN-DPCC
Source: Authors, (2025).

The fast Fourier transform (FFT) harmonic spectrums for both scenarios, with a fundamental frequency of 50 Hz, are shown in Figure 8. The phase-A currents of each system are subjected to a FFT analysis to assess further the impact of the per cent distortion on current quality. Table 4 and Figure 9 present the detailed results. The proposed approach significantly improves performance when comparing PI-DPCC and ANN-DPCC control techniques with and without dead-time compensation. The phase current's THD without dead-time compensation is 11.21% for ANN-DPCC and 13.29% for PI-DPCC. However, when dead-time compensation is included, the THD significantly drops to 9.42% for PI-DPCC and 8.08% for ANN-DPCC. This illustrates how well ANN-DPCC reduces current distortion, with 28.99% and 27.91% reductions, respectively.

Table 4: THD of phase current without dead time compensation and with compensation.

Switching frequency	Methods	THD without compensation	THD with compensation	Improvement (%)
20 kHz	PI-DPCC	13.29	9.42	28.99
	ANN-DPCC	11.21	8.08	27.91

Source: Authors, (2025).

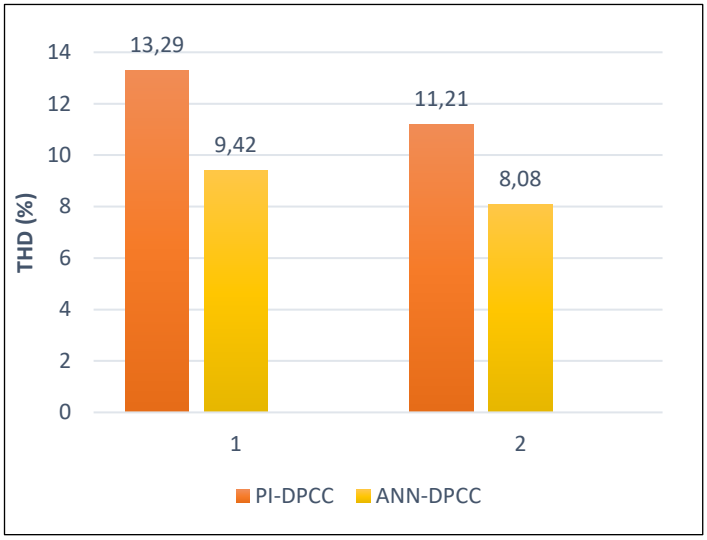

Figure 9. Total harmonic distortion comparison.
Source: Authors, (2025).

V. AUTHOR'S CONTRIBUTION

Conceptualization: Amira Slimani, Amor Bourek, Abdelkarim Ammar, Khoudir Kakouche, Wassila Hattab and Marah Bacha.
Methodology: Amira Slimani, Amor Bourek, Abdelkarim Ammar, Khoudir Kakouche, Wassila Hattab and Marah Bacha.
Investigation: Amira Slimani, Amor Bourek, Abdelkarim Ammar, Khoudir Kakouche, Wassila Hattab and Marah Bacha.
Discussion of results: Amira Slimani, Amor Bourek, Abdelkarim Ammar, Khoudir Kakouche, Wassila Hattab and Marah Bacha.
Writing – Original Draft: Amira Slimani, Amor Bourek, Abdelkarim Ammar, Khoudir Kakouche, Wassila Hattab and Marah Bacha.
Writing – Review and Editing: Amira Slimani, Amor Bourek, Abdelkarim Ammar, Khoudir Kakouche, Wassila Hattab and Marah Bacha.
Resources: Amira Slimani, Amor Bourek, Abdelkarim Ammar, Khoudir Kakouche, Wassila Hattab and Marah Bacha.
Supervision: Amira Slimani, Amor Bourek, Abdelkarim Ammar, Khoudir Kakouche, Wassila Hattab and Marah Bacha.
Approval of the final text: Amira Slimani, Amor Bourek, Abdelkarim Ammar, Khoudir Kakouche, Wassila Hattab and Marah Bacha.

VI. CONCLUSIONS

The proposed Deadbeat Predictive Current Control strategy, enhanced with an ANN-based speed controller and integrated dead-time compensation, demonstrates significant advancements in the control of PMSMs. The system achieves superior dynamic performance, adaptability to load variations, and improved reference speed tracking by replacing traditional PI controllers with ANN in the speed outer loop. The integration of dead-time compensation effectively mitigates the voltage distortions and current ripples caused by switching delays in the inverter, reducing harmonic distortion and enhancing overall efficiency. The simulation results validate the effectiveness of this approach, highlighting its potential for improving the reliability and performance of PMSM drives in modern applications.

VII. REFERENCES

[1] T. Li, X. Sun, G. Lei, Y. Guo, Z. Yang, and J. Zhu, "Finite-control-set model predictive control of permanent magnet synchronous motor drive systems—An

overview," IEEE/CAA J. Autom. Sinica, vol. 9, no. 12, pp. 2087–2105, 2022. doi: 10.1109/JAS.2022.105851.

[2]cK. Kakouche, W. Guendouz, T. Rekioua, S. Mezani, and T. Lubin, "Application of fuzzy controller to minimize torque and flux ripples of PMSM," in Proc. Int. Conf. Adv. Electr. Eng. (ICAEE), Algiers, Algeria, Nov. 19–21, 2019. doi: 10.1109/ICAEE47123.2019.9015066.

[3] Z. Zhang, H. Li, S. Zhou, and Z. Li, "An effective adaptive-observer based wide range encoderless control for PMSM drives," IEEE Trans. Ind. Electron., pp. 1–13, 2023. doi: 10.1109/TIE.2023.3337539.

[4] J. Rodriguez et al., "Latest advances of model predictive control in electrical drives—Part I: Basic concepts and advanced strategies," IEEE Trans. Power Electron., vol. 37, no. 4, pp. 3927–3942, 2022. doi: 10.1109/TPEL.2021.3121532.

[5] A. Ammar, B. Talbi, T. Ameid, Y. Azzoug, and A. Kerrache, "Predictive direct torque control with reduced ripples for induction motor drive based on T-S fuzzy speed controller," Asian J. Control, vol. 21, no. 4, pp. 2155–2166, 2019. doi: 10.1002/asjc.2148.

[6] M. S. Rafaq, W. Midgley, and T. Steffen, "A review of the state of the art of torque ripple minimization techniques for permanent magnet synchronous motors," IEEE Trans. Ind. Informat., vol. 20, no. 1, pp. 1019–1031, 2023. doi: 10.1109/TII.2023.3272689.

[7] D. Liu, Y. Fan, J. Liu, G. Wang, and L. Sheng, "Robust deadbeat predictive current control for unipolar sinusoidal excited SRM with multi-parameter mismatch compensation," Sci. Rep., vol. 14, no. 1, p. 23746, 2024. doi: 10.1038/s41598-024-73517-2.

[8] M. Sahin, "Optimization of model predictive control weights for control of permanent magnet synchronous motor by using the multi objective bees algorithm," in Model-Based Control Engineering—Recent Design and Implementations for Varied Applications, 2021. doi: 10.5772/interchopen.98810.

[9] X. Liu, L. Qiu, Y. Fang, K. Wang, Y. Li, and J. Rodríguez, "Finite control-set learning predictive control for power converters," IEEE Trans. Ind. Electron., vol. 717, pp. 8190–8196, 2024, doi: 10.1109/TIE.2023.3303646.

[10] A. Slimani, A. Ammar, A. Burek, K. Kakouche, W. Hattab, and B. Marah, "Model predictive current controlled PMSM drive with fuzzy logic for electric vehicle applications," in 2nd IEEE Int. Conf. Electr. Eng. Autom. Control (ICEEAC), Sétif, Algeria, May 12–14, 2024. doi: 10.1109/ICEEAC61226.2024.10576506.

[11] S. Dai, J. B. Wang, Z. Sun, and E. Chong, "Deadbeat predictive current control for high-speed PMSM drives with low switching-to-fundamental frequency ratios," IEEE Trans. Ind. Electron., vol. 69, no. 5, pp. 4510–4521, May 2022. doi: 10.1109/TIE.2021.3078383.

[12] Y. Wang, Z. Li, S. Zhou, Y. Zhang, J. Zhang, H. Li, and Z. Zhang, "An enhanced deadbeat predictive current control for high-speed PMSM drives," in 2024 IEEE 10th International Power Electronics and Motion Control Conference (IPEMC-ECCE Asia), May 2024, pp. 2741–2746. doi: 10.1109/IPEMC-ECCEAsia60879.2024.10567942.

[13] X. Qu, Q. Wang, C. Peng, and Z. Li, "Novel deadbeat direct torque and flux control for interior permanent magnet synchronous motor," Electr. Eng., pp. 1–10, 2024. doi: 10.1007/s00202-024-02606-2.

[14] Y. Yao, Y. Huang, F. Peng, J. Dong, and H. Zhang, "An improved deadbeat predictive current control with online parameter identification for surface-mounted PMSMs," IEEE Trans. Ind. Electron., vol. 67, no. 12, pp. 10145–10155, 2020. doi: 10.1109/TIE.2019.2960755.

[15] X. Wang, Y. Zhang, and H. Yang, "An improved deadbeat predictive current control for induction motor drives," IET Power Electron., vol. 16, no. 1, pp. 1–10, 2023. doi: 10.1049/pel2.12358.

[16] X. Yuan, S. Zhang, and C. Zhang, "Enhanced robust deadbeat predictive current control for PMSM drives," IEEE Access, vol. 7, pp. 148218–148230, 2019. doi: 10.1109/ACCESS.2019.2946972.

[17] J. Liu and H. Chen, "Dead-time compensation for PMSM with phase shift of impedance considered based on adaptive linear neuron method," IET Electr. Power Appl., 2024. doi: 10.1049/elp2.12463.

[18] C. Xia, B. Ji, and Y. Yan, "Smooth speed control for low-speed high-torque permanent-magnet synchronous motor using proportional–integral resonant controller," IEEE Trans. Ind. Electron., vol. 62, no. 4, pp. 2123–2134, 2015. doi: 10.1109/TIE.2014.2354593.

[19] Y. Wang, W. Liao, S. Huang, J. Zhang, M. Yang, C. Li, and S. Huang, "A robust DPCC for IPMSM based on a full parameter identification method," IEEE Trans. Ind. Electron., vol. 70, no. 8, pp. 7695–7705, 2022. doi: 10.1109/TIE.2022.3212371.

[20] A. Ammar, O. Belaroussi, M. Benakcha, A. Zemmit, and T. Ameid, "Super-Twisting MRAS observer-based non-linear direct flux and torque control for induction motor drives," Power Electron. Drives, vol. 9, pp. 374–396, 2024. doi: 10.2478/pead-2024-0024.

[21] D. Karboua, Y. Chouiha, B. O. Douara, I. F. Bouguenna, S. Benkaihoul, and B. Toual, "Advanced dual-loop control architecture for superior PMSM performance utilizing finite-control-set model predictive control and exponential reaching law sliding mode control," ITEGAM-JETIA, vol. 10, no. 49, pp. 71–79, 2024. doi: 10.5935/jetia.v10i49.1221.

[22] K. Kakouche, A. Oubelaid, S. Mezani, D. Rekioua, and T. Rekioua, "Different control techniques of permanent magnet synchronous motor with fuzzy logic for electric vehicles: Analysis, modelling, and comparison," Energies, vol. 16, no. 16, p. 3116, 2023. doi: 10.3390/en16073116.

[23] Y. Xu, S. Li, and J. Zou, "Integral sliding mode control-based deadbeat predictive current control for PMSM drives with disturbance rejection," IEEE Trans. Power Electron., vol. 37, no. 3, pp. 2845–2856, 2021. doi: 10.1109/TPEL.2021.3115875.

[24] S. Y. Kim and S. Y. Park, "Compensation of dead-time effects based on adaptive harmonic filtering in the vector-controlled AC motor drives," IEEE Trans. Ind. Electron., vol. 54, no. 3, pp. 1768–1777,2007. doi: 10.1109/TIE.2014.2354593.

[25] L. Buchta and L. Otava, "Compensation of dead-time effects based on Kalman filter for PMSM drives," IFAC-PapersOnLine, vol. 51, no. 6, pp. 18–23, 2018. doi: 10.1016/j.ifacol.2018.07.123.

[26] M. Yessef, H. Benbouhenni, M. Taoussi, A. Lagrioui, I. Colak, S. Mobayen, and B. Bossoufi,"Real-time validation of intelligent super-twisting sliding mode control for variable-speed DFIG using dSPACE 1104 board," IEEE Access, 2024. doi: 10.1109/ACCESS.2024.3367828.

[27] S. Mahfoud, A. Derouich, and N. El Ouanjli, "Performance improvement of DTC for doubly fed induction motor by using artificial neuron network," in Int. Conf. Digital Technol. Appl., Cham: Springer Int. Publishing, pp. 32–42, 2022. doi: 10.1007/978-3-031-02447-4_4.